

Design and analysis of the novel plasmonic split ring resonator power splitter appropriate for photonic integrated circuits

ESMAT RAFIEE, ROOZBEH NEGAHDARI, FARZIN EMAMI*

Optoelectronic Research Center, Electronic Department, Shiraz University of Technology, Shiraz, Iran

In this paper, a novel MIM split ring resonator power splitter has been designed and analyzed. This resonator is coupled to three T-shaped waveguides. Simulations are done based on FDTD method. Split ring and T-shaped waveguides are made of air; which are situated in silver-background. The electromagnetic wave is applied to split ring through input port and in specific wavelengths is transmitted to individual output ports. The normalized transmitted powers are up to approximately 0.85; which are so desirable. Effects of structural parameters on the transmission power are also considered. In this structure lightwave can be confined to sub-wavelength dimensions.

(Received February 5, 2018; accepted April 8, 2019)

Keywords: MIM structure, Power splitter, Split ring resonator, Surface plasmon polariton (SPP)

1. Introduction

As known, electronic integrated circuits (EIC) are continuously shrinking in dimensions according to Moore's law [1]. If designing small scaled photonic integrated circuits (PIC) like EICs is considered, decreasing the size of the photonic waveguides and other optical devices would be also essential [1]. Integrating the optical circuits resulting in miniaturizing the size, increasing the speed and improving the performance of the optical devices has attracted great attentions in recent years. Basic obstacles for diminishing the size of the current optical devices are the optical diffraction limits and great optical losses [2].

One of the most practical ways to guide lightwave at a subwavelength scaled devices is to use a surface plasmon polaritons (SPP) at the boundary of a noble metal and a dielectric [1]. In fact, plasmonics establish the interesting field in nano-photonics by confining electromagnetic fields in nano-meter dimensions (below the operating wavelength).

The interaction between electromagnetic radiations and free electrons at metal-insulator interfaces lead to the excitation of surface plasmon polaritons. Surface plasmon polaritons are appropriate candidates to conquer the diffraction limit and allow the lightwave to be propagated in the nanoscale devices and PICs. As stated, surface plasmons are electromagnetic excitations that propagate through metal-dielectric interfaces and create new structures which can confine light into sub-wavelength regions [3-6]. The SPP energy is properly confined over the surface and is decayed exponentially in the normal directions of both media (metal and insulator) [7-9]. Propagating surface plasmon polaritons is intensely

sensitive to the geometries and surrounding medium of the structures.

Ring resonators are important components in integrated circuits; being utilized in compact optical circuits. Plasmonic ring resonators can be used in highly integrated optical circuits [9-14]. Split rings are established by positioning a strip in the ring environment. Split rings can support multipolar resonances better than simple rings and can be adjusted by the split angle instead of different structural parameters [13,15].

Insulator-metal-insulator (IMI) and metal-insulator-metal (MIM) structures are the two most important geometries for plasmonic waveguides. IMI structures can carry lightwaves in a long distance but their light confinement is poor due to the dielectric cladding layers [3]. In the MIM configurations, the lightwave is propagated through the dielectric medium in the subwavelength dimensions with high confinement.

Although, as the metal claddings generate higher losses, the propagation length of MIM waveguides is lower compared to IMI waveguides; its amount is sufficient for nano-photonics applications [3-7].

Therefore, the MIM split-ring structures are better choices for PIC circuits compared to IMI structures, as they have stronger confinement of light. Additionally, MIM split-ring resonators can support multi-polar plasmonic resonances better than simple rings; establishing structures with multi-channel applications. It is known that, in MIM split ring, plasmonic resonances with odd modes can be obtained, when the polarization of incident field is perpendicular to the split of the ring. On the other hand, even resonance modes are excited if the polarization of the incident field is parallel to the split [14, 16].

In order to increase the lateral confinement and sensitivity of the proposed structure and decreasing the absorption loss in the MIM resonator, longer coupling regions are required. This requirement is fulfilled by using T-shaped waveguides. These waveguides increase lateral interaction length and coupling efficiencies [17]. Therefore the combination of split ring resonator and T-shaped waveguides is of great interest.

Surface plasmon polaritons can be utilized in different structures for different applications. Some of SPP-based nano-phonic devices, such as filters [18, 19], couplers [20], sensors [17,21,22] and logic gates [23], have been proposed recently.

Power splitters (PS) are the most regularly used power division devices, and are prominent components in PICs. A need for highly dense PICs has raised the necessities to have greatly compact power splitters. These compact PSs can be modified by SPP-based nano-phonic structures. Some of the SPP-based power splitters were fabricated and their experimental results were presented in [1, 2, 24].

In a research [25], a plasmonic dichroic splitter based on periodic metallic nanoslits was proposed and investigated. The incident light at two different wavelengths was coupled into plasmons propagating in the structure. It was indicated that the good coupling and splitting performances with coupling efficiencies of 0.5 and 0.46, splitting ratios of 26.4 dB and 21.7 dB at wavelength 1310 nm and 1550 nm were achieved for right and left side of the structure, respectively [25].

In another research [26], devices like filter, mode separator and power splitter were designed by using the theoretical relation between the resonance frequency of the nanocavities and the structural parameters. The proposed structures could be fabricated by nanostructure fabrication methods and were usable in photonic integrated circuits because of their 90° bends. Their efficiencies were less than 70% [26].

In [27], a mid-infrared plasmonic power splitter using an analytic approach was proposed. For achieving plasmonic effects in mid-infrared region, Doped Silicon was utilized. By using the proposed technique, 1x4, 1x8 and 1x12 power splitters with wide bands in the MIR and negligible imbalances could be obtained. The efficiency was about 60% [27].

In [28] a dual-band power splitter based on the base of nontraditional asymmetrical reentrant configuration was

proposed. In the proposed structure, two adjacent work bands were created, improving the weight, size, compatibility and cost of the splitter. The splitter could be utilized in photonic integrated circuits with efficiency of 65% [28].

In our previous work [14], a plasmonic-dielectric power splitter-filter based on two dimensional photonic crystals was designed and simulated. The structure contained air, Al, Ag and Cu rods in Si background. The acceptable TM PBG in the wavelength range of $1.055\mu\text{m} < \lambda < 1.266\mu\text{m}$ was obtained. The functionality of the structure as a power splitter was defined with efficiency of about 60% [14].

In this paper, performance of a novel MIM plasmonic power splitter with two output ports has been analyzed and simulated by the finite-difference time-domain (FDTD) numerical method. The proposed structure can confine light to sub-wavelength dimensions; could be utilized in photonic integrated circuits (PICs). By investigating the effects of different structural parameters, the improved structure is finally proposed. In Section 2, the structure and simulation method are presented. In Section 3, the results of the analysis and simulation of the plasmonic power splitter, are described and discussed. The conclusion of the article is presented in Section 4.

2. Structure and simulation method

The proposed plasmonic power splitter is consisted of a split ring resonator and three T-shaped waveguides. For the analysis, the FDTD numerical method, as a general and powerful method for calculating the electromagnetic field distributions in plasmonic structures, has been employed to the structure. The split ring resonator coupled to three T-shaped waveguides can be seen in Fig. 1. The purple and gray areas denote *air* and *Ag*, respectively.

The structural parameters defined in Fig. 1 are tabulated in Table 1. Three individual ports are shown in Fig. 1, defined as input, output 1 and output 2 ports.

A plane wave is launched to the split ring through the left T-shaped waveguide (input port), (exciting surface plasmonic resonances), then the transmitted resonant waves are monitored from the down (output1) and top (output2) T-shaped waveguides.

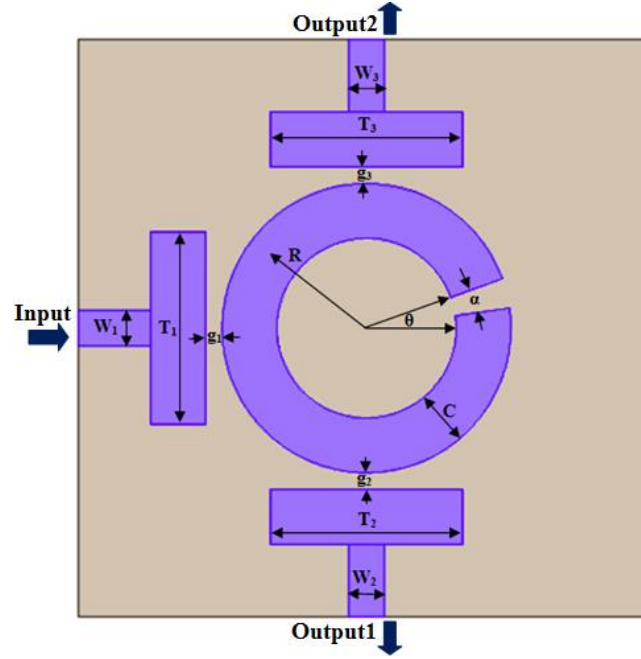


Fig. 1. The proposed plasmonic power splitter

Table 1. The appropriate structural parameters

Parameter definition	Parameter value
W_1 (width of the left waveguide)	10 nm
W_2 (width of the down waveguide)	4 nm
W_3 (width of the top waveguide)	8.5 nm
T_1 (length of the left waveguide)	140 nm
T_2 (length of the down waveguide)	130 nm
T_3 (length of the top waveguide)	95 nm
g_1 (distance between left waveguide and ring)	0.21 nm
g_2 (distance between down waveguide and ring)	0.15 nm
g_3 (distance between top waveguide and ring)	1 nm
θ	-44°
α	5°
R (average ring radius)	106.6 nm
C (ring thickness)	50 nm

As depicted in Fig. 1, split ring resonator is a fundamental block of this system. As known, ring resonators have attracted extensive attentions in recent years due to their compactness, high quality factor, and simplicity of fabrication [10, 11]. Therefore, explaining their functionality is necessary and essential. According to the eigenvalue relation for ring resonators, the resonance wavelength λ_0 can be obtained by using the refractive index of the material and the radius of the ring resonator [10, 11].

Theoretically, the resonance wavelength of the ring resonator can be obtained by the following equation [16]:

$$\frac{J'_n(kr_2)}{J'_n(kr_1)} - \frac{N'_n(kr_2)}{N'_n(kr_1)} = 0 \quad (1)$$

where $k = \omega\sqrt{\epsilon_0\epsilon_r\mu_0}$, μ_0 and ϵ_r are air permeability and frequency-dependent effective relative permittivity, respectively. J_n and N_n are the first and second Bessel functions with the order n respectively. J'_n and N'_n are derivatives of the Bessel functions to the argument kr .

From equation (1), the resonance wavelength λ_0 can be

obtained due to the refractive index of the material and the radius of the ring resonator. Once a particular radius is selected, the resonance wavelengths would be dependent to the refractive indices [16]. To indicate this feature, the resonant wavelength of an MIM ring resonator can be approximated as follow [10, 11]:

$$\lambda_r = \frac{mc}{rn_{eff}} \quad (2)$$

in which, m is a positive integer indicating the resonant mode number, c is the free-space speed of light and $r \equiv \frac{r_i + r_o}{2}$ is defined as the average radius of the ring [10, 29].

By inserting a strip within the ring, a split ring resonator would be established. In the split ring resonator, the resonance frequencies are highly regulable by adjusting the geometric parameters of the ring [9]. The MIM split-ring structures are better choices for PIC circuits compared with IMI structure, as they can highly confine the light. Actually, MIM split-ring resonators can support multipolar plasmonic resonances better than simple rings; establishing Multichannel filters. In MIM split ring, plasmonic resonances with odd modes can be achieved, when the polarization of incident field is perpendicular to the split of the ring. On the other hand, even resonance modes are excited if the polarization of the incident field is parallel to the split [9]. Thus, we can approximate split rings with perfect rings by little tolerances.

As indicated in Fig. 1, the structure is consisted of Ag and *air*. The frequency-dependent complex relative permittivity of silver can be characterized by the Drude mode [29-31]:

$$\varepsilon_m(\omega) = \varepsilon_\infty - \omega_p^2 / (\omega(\omega + i\gamma)) \quad (3)$$

where the bulk plasma frequency of free conduction electrons (ω_p) is 9.1 eV , the electron collision frequency (γ) is 0.018 eV , (ω) is the angular frequency of the incident electromagnetic radiation and the dielectric constant at infinite frequency (ε_∞) is 3.7 [29-31]. In the simulations,

the perfectly matched layers (PML) are employed around the system; in order to prevent reflection from the output ports [10, 11].

3. Simulation results and discussions

For describing the functionality of the proposed structure, the incident EM field is launched to the input port. Each output port resonates at specific wavelengths. The amount of power transferred to each port is also different. In fact, in definite wavelengths the down and top T-shaped waveguides are resonated, indicating the power splitting process. In this research, at resonance wavelengths of output1 and output2 ports, transmission and field distribution spectra are achieved. For improving the functionality of the system, effects of length and width of each output waveguide on the peak value of transmission spectrum are also investigated and analyzed. In the next section, power splitting at two output ports is studied.

3.1. Power splitting in Output 1

In the first step, EM wave is launched to the input port. Incident signal is coupled to the split ring through the input port. At $\lambda=1.08 \mu\text{m}$, the circulating filed in the split ring would be coupled to the down T-shaped waveguide. In this wavelength, the signal is transferred to the output 1 port, indicating both the filtering and power splitting functionalities of the proposed structure. The field distribution spectrum at this wavelength can be seen in Fig. 2 a.

The transmission spectrum is also shown in Fig. 2 b. As can be seen, the transmission power reaches 0.75 at $\lambda=1.08 \mu\text{m}$. This value is acceptable for the amount of transmitted power in the output port. Therefore, the structure's functionality at this wavelength would be desirable. In this wavelength, output 1 can transfer the signal, indicating high transmission power. In the next part, the power splitting operation at output 2 would be indicated.

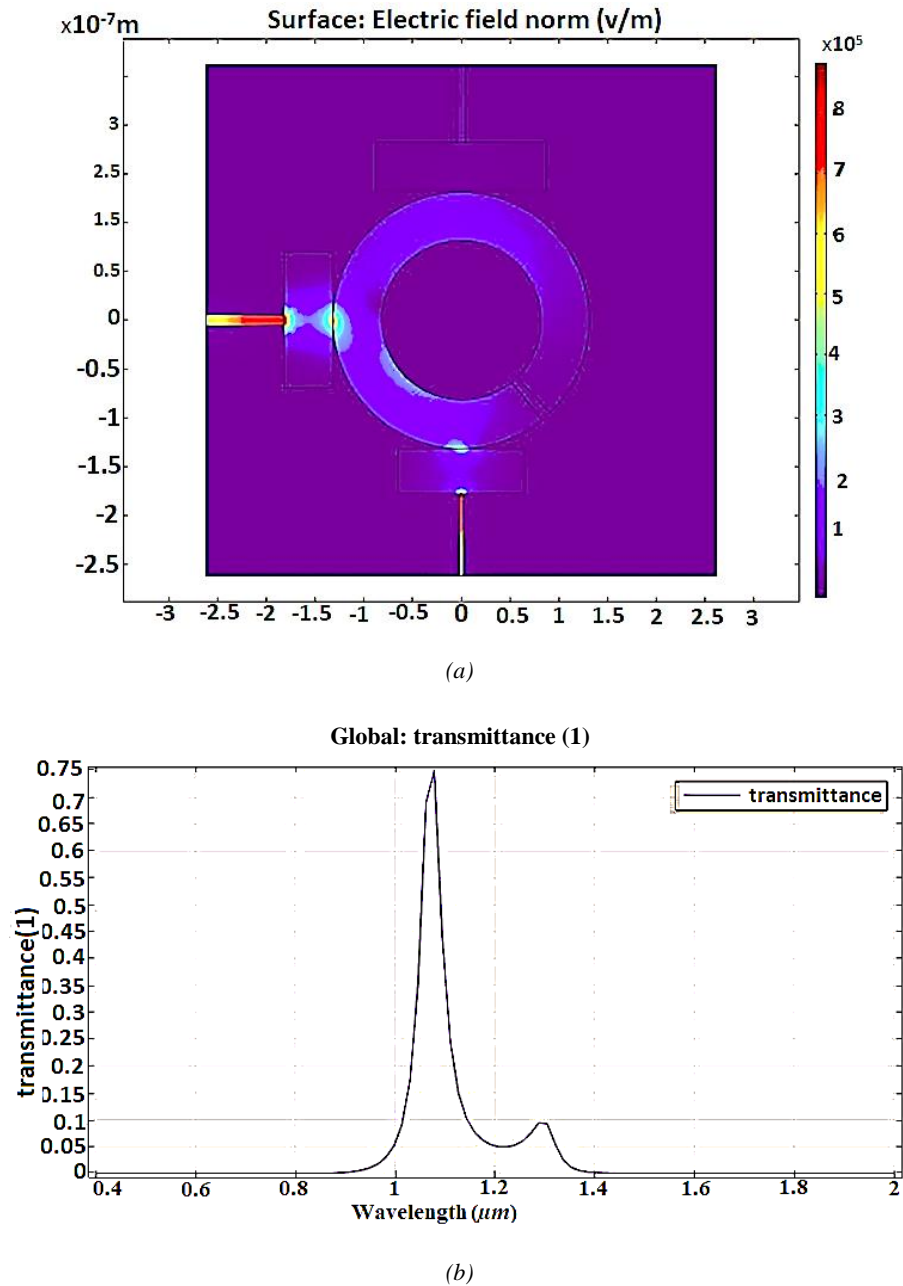
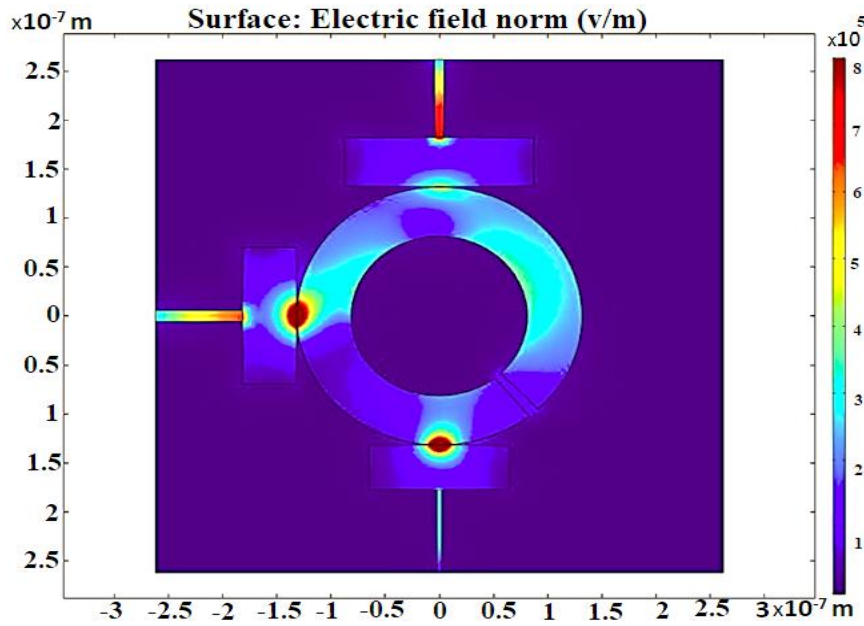


Fig. 2. a) Field distribution in the plasmonic ring resonator power splitter, b) Transmission spectrum of the split-ring resonator power splitter at $\lambda=1.08 \mu\text{m}$ in Output 1

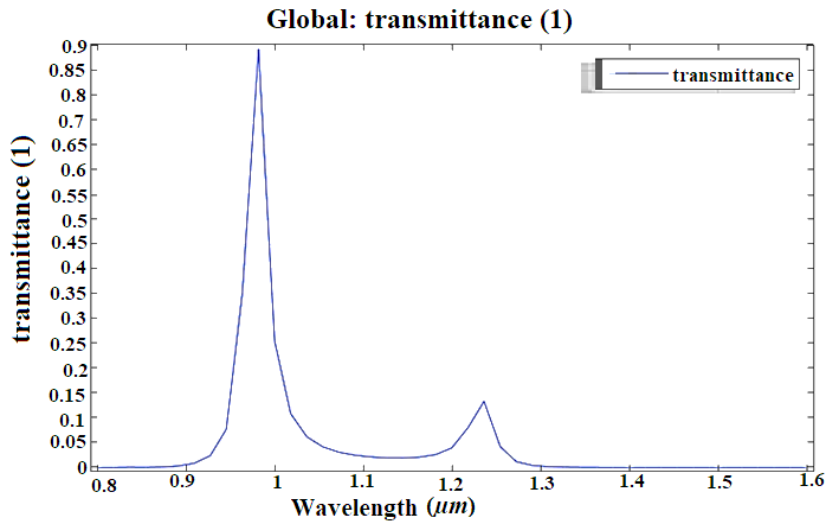
3.2. Power splitting in Output2

As the incident field is propagated in the split ring, at $\lambda=0.97 \mu\text{m}$, it would be coupled to the top T-shaped waveguide.

In this wavelength, the signal is transferred to the output 2 port, exhibiting both the filtering and power splitting functionalities of the proposed structure. The field distribution spectrum at this wavelength can be depicted in Fig. 3 a.



(a)



(b)

Fig. 3. a) Field distribution in the plasmonic ring resonator power splitter, b) Transmission spectrum of the split-ring resonator power splitter at $\lambda=0.97 \mu\text{m}$ in Output 2

The transmission spectrum at this wavelength is shown in Fig 3.b. As can be concluded, the transmission power reaches 0.85 at $\lambda=0.97\mu\text{m}$. This figure indicates transferring the desirable amount of the signal to output 2 port. Therefore, the structure's functionality at this wavelength would be desirable. By considering these two cases, the proposed structure can be presented as a two port power splitter.

The functionality of the proposed power splitter can be improved by adjusting the transmission peak to its highest available amount. Therefore to promote the properties of the proposed structure, effects of different structural parameters on output 1 and output 2 are studied.

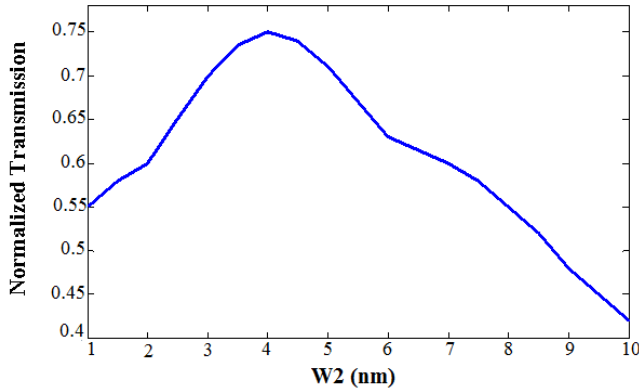
For this purpose, in each case effects of one parameter are studied while others are kept constant. Then, the variation of the normalized transmission with respect to the variable parameter would be depicted. The results are presented in the next section [14].

3.3. Effects of structural parameters

In this section effects of the widths and lengths of the top and down waveguides on the normalized transmission power for output 1 and output 2 ports, are investigated. By doing so, the best parameters for the improved structure can be obtained.

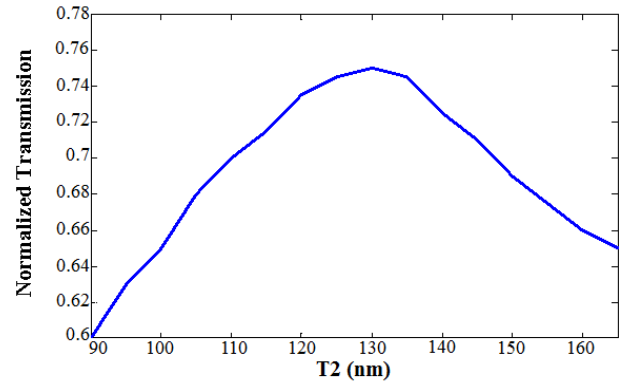
a) Effects of W_2 and T_2

In the first step, effects of W_2 and T_2 are considered for the results of output 1. The parameter " W_2 " is changed



(a)

between 1nm to 10nm, with the results being shown in Fig 4 a. Then, parameter W_2 would be considered at its best value and parameter " T_2 " would be varied between 90nm to 165nm and shown in Fig 4 b.



(b)

Fig. 4. (a) Effects of W_2 on the normalized transmission power, (b) Effects of T_2 on the normalized transmission power

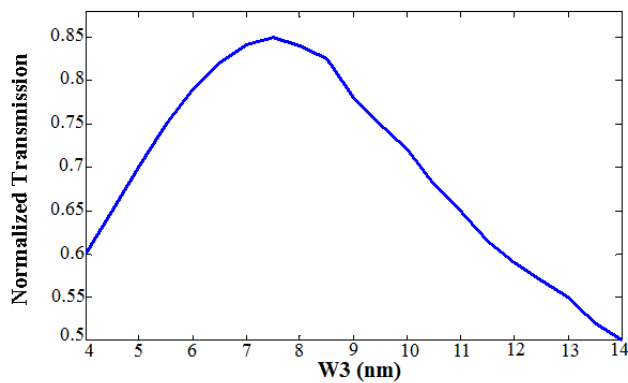
As can be seen in Fig. 4 a, there would be an optimum value for the transmission peak power in the middle of the spectrum at $W_2=4$ nm, where the transmission power equals 0.755. It can be suggested that the evanescent fields become stronger if " W_2 " is diminished from 10nm to 4nm; this phenomenon increases the coupling coefficient. In another case, if " W_2 " is increased from 1nm to 4nm, the transmission power becomes stronger. This phenomenon occurs due to the coupling coefficient enhancement. In fact, larger waveguide widths ensure smaller attenuation coefficients of the waveguide, especially for bending regions of the waveguide [10, 11]; since a larger waveguide width provides a stronger optical confinement to prevent the ring from suffering considerable optical loss (attenuation) in the bending regions [10,11-14], [32], [33]. Therefore its best value is situated in the middle of the spectrum [14].

In the next case as can be seen from Fig. 4 b, effects of " T_2 " are considered. As known, the coupling region has a major effect on the performance of the structure; which is a T-shaped waveguide in this system. The coupling length

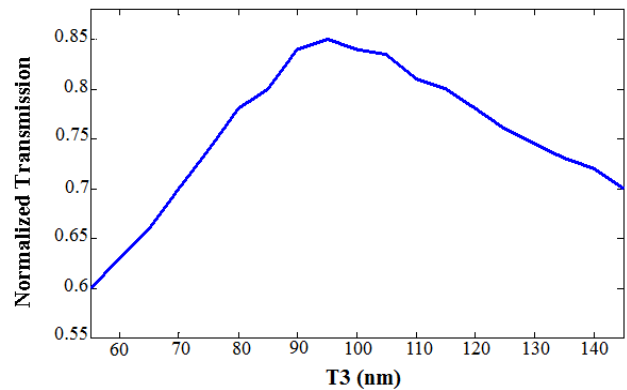
mostly depends on the dielectric constants of the metal and the geometry of the power splitter. Therefore " T_2 " has a great effect on the performance of the structure [34]. As " T_2 " is increased from 90nm to 130nm, the coupling length is increased, improving the transmission power. On the other hand, by increasing " T_2 " from 130nm to 165nm, transmission peak is decreased; due to the higher confinement of signal. Therefore its best value would be 130nm with the peak of about 0.76. It should be noted that, in larger dimensions of length and width, signal can't be propagated towards Output 1 [9,10,11], [35,36, 37].

(b) Effects of W_3 and T_3

In the next step, effects of W_3 and T_3 are investigated for the results of Output 2. The parameter " W_3 " is changed between 4nm to 14nm, with the results being depicted in Fig. 5 a. Then, parameter W_3 would be chosen at its best value and parameter " T_3 " would be varied between 55nm to 145nm and shown in Fig. 5 b.



(a)



(b)

Fig. 5. (a) Effects of W_3 on the normalized transmission power, (b) Effects of T_3 on the normalized transmission power

As can be seen from Fig. 5 a, there would be an optimum value for the transmission peak power in the middle of the spectrum at $W_3=7.5\text{nm}$, where the transmission power equals 0.855. It is indicated in Fig. 5 b, that the best value for T_3 would be 95nm with the peak of about 0.86. All the discussions presented for the reason of variations of T_2 and W_3 can be considered for T_3 and w_3 as well. It should also be noted that, in larger dimensions of length and width, signal can't be propagated towards Output 2.

4. Conclusions

In this research, a novel MIM plasmonic split ring resonator power splitter was designed and simulated. Split ring resonator and T-shaped waveguides were made of air in silver background. The electromagnetic waves were applied to the split ring through input port and transmitted to output 1 and output 2. It was shown in the simulations that for specific wavelengths, only one output port gains high power value; indicating power splitter operation. At $\lambda=1.08$ the signal was coupled to the down T-shaped waveguide with the value of 0.75, and at $\lambda=0.97\mu\text{m}$ it was coupled to the top T-shaped waveguide with 0.85 power value. Effects of the width and lengths of T-shaped waveguides on the normalized transmission power were also considered for improving the performance of the system. As suggested, in this structure lightwaves can be confined to sub-wavelength dimensions (of the order of nano meter); being appropriate for highly optical integrated circuits.

References

- [1] Z. Han, S. He, Opt. Commun. **278**, 199 (2007).
- [2] N. Nozhat, N. Granpayeh, Opt. Commun. **284**, 3449 (2011).
- [3] W. Cai, W. Shin, Adv. Mater. **22**, 5120 (2010).
- [4] H. Choo et al., Nature Photon. **6**, 838 (2012).
- [5] A. Eshaghian et al., J. Opt. Soc. Am. B **31**, 458 (2014).
- [6] M. Bahador et al., J. of Lightwave Tech. **32**, 2659 (2014).
- [7] S. A. Maier, Plasmonics: Fundamentals and Applications, Springer, Bath, UK 2007.
- [8] D. K. Gramotnev, S. I. Bozhevolnyi, Nature Photon. **4**, 83 (2010).
- [9] K. J. Chen et al., IEEE Photon. J. **6**, 2200207 (2014).
- [10] E. Rafiee, F. Emami, N. Nozhat, Opt. Eng. **53**, 123108 (2014).
- [11] E. Rafiee, F. Emami, Optik. **127**, 1690 (2016).
- [12] M. Janipour et al., J. of Electro. Anal. and App. **5**, 405 (2013).
- [13] D. Lehr et al., Opt. Lett. **37**, 157 (2012).
- [14] E. Rafiee, Optik **172**, 534 (2018).
- [15] D. Liu, Opt. Exp. **17**, 2906 (2009).
- [16] T. B. Wang et al., Opt. Exp. **17**, 24096 (2009).
- [17] X. Wang et al., J. Appl. Phys. **107**, 124517 (2010).
- [18] I. Zand et al., IEEE Photon. J. **4**, 2136 (2012).
- [19] Y. Gong et al., Opt. Lett. **35**, 285 (2010).
- [20] Z. Han et al., Opt. Commun. **259**, 690 (2006).
- [21] N. Nguyen-Huu et al., IEEE Photon. J. **5**, 2700108 (2013).
- [22] X. Ren et al., App. Opt. **56**, H1 (2017).
- [23] Z. Chen et al., IEEE Photon. Technol. Lett. **24**, 1366 (2012).
- [24] B. Chen, C. Liu, Opt. Commun. **355**, 367 (2015).
- [25] C. C. Ho et al., Opt. Commun. **355**, 591 (2015).
- [26] A. Dolatabady et al., IET Opt. J. **9**, 289 (2015).
- [27] M. A. Ayad, IEEE Photon. Tech. Lett. **28**, 16372965 (2016).
- [28] V. V. Atuchin, Int. J. Electron. Commun. **84**, 21 (2018).
- [29] A. D. Rakic, A. B. Djurišić, J. M. Elazar, M. L. Majewski, App. Opt. **37**, 5271 (1998).
- [30] Z. Han et al., IEEE Photon. Technol. Lett. **19**, 91 (2007).
- [31] T. Zentgraf et al., Phys. Rev. B, Condens. Matter **76**, 033407 -1 (2007).
- [32] Z. Wei et al., Photon. and Nanostruc. **23**, 45 (2016).
- [33] H. Xu, H. Li, G. Xia, Q. Chen, Opt. Commun. **377**, 70 (2016).
- [34] N. Nozhat et al., Photonics Global Conference (PGC), Singapore, 2010.
- [35] X. Li, Z. Wei, Y. Liu, N. Zhong, X. Tan, Phys. Lett. A **380**, 232 (2016).
- [36] E. Rafiee, F. Emami, Optik **140**, 873 (2017).
- [37] E. Rafiee et al., J. of Electromag. Waves and App. **32**, 1925 (2018).

*Corresponding author: emami@sutech.ac.ir